Amyloid Morphology is Encoded in H-bonds and Electrostatics Interactions Ruling Protein Phase Separation

Samuel Lenton,[†,‡,¶] Hussein Chaaban,[†,‡,¶] Mohammed Khaled,[†,§] Marco van de Weert,[‡,¶] Birgit Strodel,[*,§,‖] and Vito Foderà[*,‡,¶]

[†]*Equal contribution*

[‡]*Department of Pharmacy, Faculty of Health and Medical Sciences, University of Copenhagen, Universitetsparken 2, 2100 Copenhagen, Denmark*

[¶]*Center for Biopharmaceuticals and Biobarriers in Drug Delivery, University of Copenhagen, Universitetsparken 2, 2100 Copenhagen, Denmark*

[§]*Institute of Biological Information Processing (IBI-7: Structural Biochemistry), Forschungszentrum Jülich, 52425 Jülich, Germany*

[‖]*Institute of Theoretical and Computational Chemistry, Heinrich Heine University Düsseldorf, 40225 Düsseldorf, Germany*

E-mail: b.strodel@fz-juelich.de; vito.fodera@sund.ku.dk

Abstract

We report the mechanisms by which H-bonds and electrostatic interactions in ion-protein systems determine phase separation and amyloid formation. Using microscopy, small-angle X-ray scattering and atomistic molecular dynamics simulations, we found that anions interacting with insulin induced phase separation by neutralising the protein charge and forming H-bonds between insulin molecules. The same interaction was

responsible for an enhanced insulin conformational stability and resistance to oligomerisation. Under aggregation conditions, the anion-protein interaction translated into the activation of a coalescence process, leading to amyloid-like microparticles. This reaction is alternative to conformationally-driven pathways, which give rise to amyloid-like fibrils and core-shell structures, and occur instead in the absence of ion-protein binding. Our findings depict a scenario in which common interactions dictated both phase separation at low temperatures and the occurrence of heterogeneity in the amyloid morphology at high temperatures, similar to what has been reported for protein crystallisation.

Introduction

Cells use membrane-enclosed organelles to selectively segregate specific biochemical reactions within isolated sub-cellular compartments; this is regulated by a process called liquid-liquid phase separation (LLPS).[1–4] In protein systems, LLPS is characterised by the formation of two distinct liquid phases, one enriched with the protein, known as the scaffold or dense phase, and one containing a lower concentration of the protein called the dilute phase.[5] Due to the highly concentrated protein phase, LLPS provides ideal conditions for the onset of nucleation processes and, eventually, liquid-to-solid transitions.[6,7]

The nucleation and growth of crystals from protein-dense phases has been reported for a number of proteins. This process has been explained by a two-step crystallisation mechanism: initially, a nucleus is formed, which undergoes metastable liquid–liquid phase separation, followed by a conformational change that results in the formation of a highly ordered crystalline phase.[8–11] This mechanism differs from classical nucleation theory, in which the nucleus is formed directly from a supersaturated solution.[12,13] LLPS may influence crystallisation outcomes, such as crystal morphology, and determine the metastable forms of crystals.[14,15]

In addition to crystallisation, and under specific destabilising conditions, the protein-dense phase can undergo a transition into semi-crystalline and gel-like phases;[16] the latter is generally referred to as aggregation. This transition has been reported for many protein con-

densates associated with neurological disorders, including FUS in ALS, Tau in Alzheimer's and alpha-synuclein in Parkinson's disease. The reaction results in the formation of so-called amyloid aggregates,[1–4] which are characterised by enrichment in beta-sheet secondary structure. This phenomenon is also related to drug stability; at the high concentrations required for formulations, certain biopharmaceuticals can also undergo LLPS, resulting in a highly concentrated metastable protein-dense phase. In general, the presence of a metastable phase is detrimental to both the stability and efficacy of biopharmaceuticals.[17] Furthermore, biopharmaceuticals can undergo amyloid transition, which can result in in vivo complications, such as the formation of the so-called insulin balls characterised by large deposits of insulin amyloid at the injection site;[18,19] this results in lower efficacy and possible immunogenic response to the active compound.

These qualities suggest a new paradigm in our understanding of the origin of protein self-assembly pathways, in which LLPS represents the key step preceding massive aggregate formation.[7] Indeed, LLPS can affect protein oligomerisation by reducing the translational entropy of proteins[20] and lead to accelerated kinetics, change in conformational dynamics, and activation of diverse aggregation pathways.[6] In the case of intrinsically disordered proteins, the formation of dense protein phases has been shown to act as a precursor for amyloid formation.[21]

Amyloid reactions are regulated by a delicate balance between the hydrophobic attraction caused by protein unfolding and the electrostatic barrier to aggregation, which modulates protein–protein interactions during the onset of amyloid formation.[22] In this context, prior to the onset of aggregation, the presence of ions in protein solutions can give rise to complex phase diagrams resulting in, for example, coacervation, liquid-liquid phase separation, and reentrant condensation.[23,24] When induced by ions, these types of phase behaviours are caused by charge neutralisation or the formation of salt bridges. Although these phase behaviours normally take place below the temperatures used for aggregation studies, their presence sheds light on the inter-protein interactions present in solution.[25] In fact, the mag-

nitude of attractive, short-range inter-protein interactions present under diluted conditions has been used to predict proteins' propensity for phase separation or crystallisation at higher protein concentrations.[26–30]

Ions from the Hofmeister series can solubilise or desolubilise proteins and stabilise or destabilise protein structure. Buell et al. showed that different anions modified protein-protein interactions, thus altering the elongation phase of the aggregation reaction.[22] Klement et al. determined that interactions of ions with proteins resulted in modification of surface tension and protein secondary structure, changing the aggregation kinetics.[31] Owczarz and Arosio showed that the kosmotropic sulphate anion could delay the aggregation of human insulin at low pH.[32] In a more recent study, we observed that different anions from the Hofmeister series dictated the final amyloid morphology formed by insulin.[33] Moreover, the anion dependency of amyloid morphology could not be described by simple charge screening, suggesting that there are more complex, anion-specific interactions that should be considered.

Here, we provide a unifying framework that connects crystallisation, protein oligomerisation and diversity of amyloid morphologies with the propensity for forming a protein-dense phase. Using microscopy, small-angle X-ray scattering and atomistic molecular dynamics simulations, we demonstrate that, in solution, the sulphate and perchlorate anions induce phase separation of insulin by specific binding to the protein. Sulphate ions also determine the oligomerisation state of insulin and, upon storage at room temperature, the crystal formation. Upon incubation at high temperatures, the ion specific binding favours a coalescence process over a purely conformation-driven aggregation, leading to the occurrence of morphologies other than elongated fibrillar structures. As in crystallisation, a protein system's propensity to undergo LLPS dictates the type of nucleation mechanisms and aggregate morphology under amyloid-forming conditions.

Results

Anions from the Hofmeister series regulate the solubility of human insulin

The solubility of human insulin at pH 2.0 was assessed by titrating the sodium salt of each anion directly into a known concentration of insulin. During titration, the sample temperature was fixed and both the absorbance in the UV region and the light scattering at 90°were recorded. When the solubility limit was reached, the insulin solution became visually turbid and this turbidity was reflected in a sudden increase in both the measured scattered intensity and the UV absorbance at 600 nm. Calculating the final concentration of both insulin and titrated anion at this point yielded the solubility diagrams shown in Fig. 1a and b. Regarding the chloride anion, no sudden changes in turbidity were observed for the concentrations of anion and insulin tested. However, for both sulphate and perchlorate, a clear boundary of solubility dependent on both the anion and insulin concentration was observed (Fig. 1a, b). Whilst investigating the insulin solutions, we also observed that solutions of certain concentrations became turbid at low temperatures (4° C) but returned to transparency after heating back to room temperature. Therefore, we also performed titration experiments at 10° C, whereupon we observed a change in solubility to lower concentrations (Fig. 1a, b).

Both perchlorate and sulphate induce temperature-dependent phase separation of insulin

To investigate the reversible nature of the temperature-induced turbidity, we measured the intensity of scattering at 90° C as a function of temperature (with 2° C steps and 3 minutes of equilibration for each step) for both the sulphate and perchlorate anion at a fixed insulin concentration (Fig. 1c and d).

For both samples, a high intensity of scattered light at low temperatures was observed to correspond to turbid solutions, which decreased upon increasing temperature, eventually

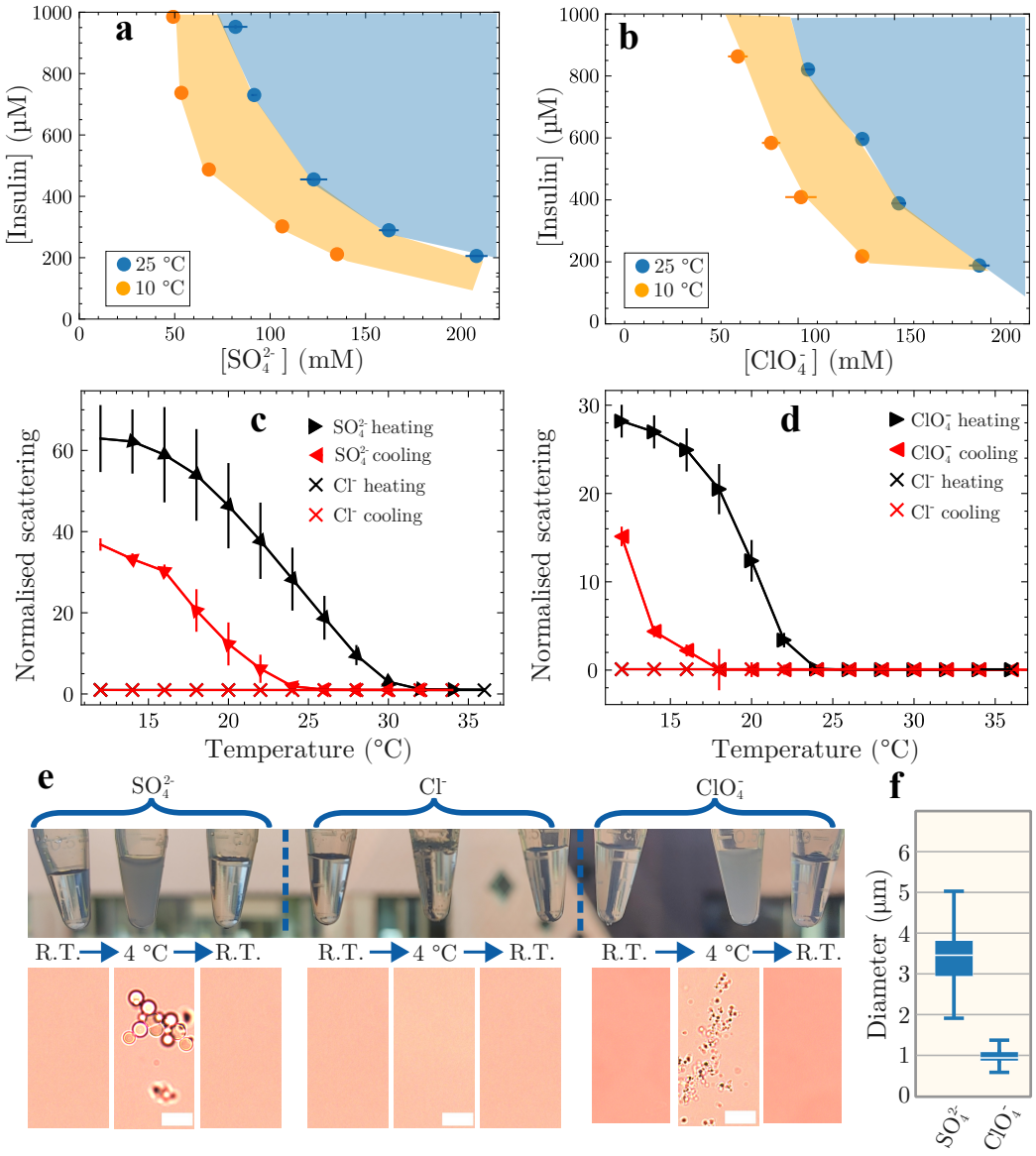

Figure 1: **(a, b)** Solubility phase diagrams as a function of insulin and anion concentrations at the indicated temperatures shown for **(a)** SO_4^{2-} and **(b)** ClO_4^-, determined by measuring scattered light intensity at a fixed angle. Shading indicates the regions of insolubility for the respective temperatures. **(c and d)** Turbidity curves of insulin (600 µM) in the presence of **(c)** 100 mM SO_4^{2-} and **(d)** 100 mM ClO_4^- shown as a function of temperature and measured by light scattering at a fixed angle. **(e)** Top row: Photographs of insulin solutions before cooling, when cooled to 4° C and upon heating back to room temperature. Bottom row: Bright-field images of the solutions under the respective conditions (scale bar=10 µm) **(f)** Size distribution of the formed coacervates (n at least 50 for both samples)

returning to a transparency. For sulphate, solutions became fully transparent at 30° C, while for perchlorate, the temperature was around 25° C. The same solutions were then cooled back down, and an increase in scattering was observed at 22° C and 17° C for sulphate and perchlorate, respectively. It should be noted that, after sufficient incubation time (15 additional minutes), both samples returned to their initially measured scattered intensity at the lowest temperature, indicating full reversibility (data not shown). The same experiment performed with 100 mM chloride showed no increase in turbidity at any of the measured temperatures (cross symbols in Figs. 1c and d). This result indicates an upper critical solution temperature (UCST)-type behaviour for insulin in the presence of 100 mM sulphate and perchlorate but not chloride.[34] The observed hysteresis between the heating and cooling curves suggests multiple interactions of the sulphate and perchlorate anions with insulin, resulting in changes of both inter- and intra-protein interactions.[34]

To investigate the causes of the observed turbidity, a single insulin sample was prepared for each anion and divided into three Eppendorf tubes. For each anion condition, one tube was kept at room temperature, while the other two were cooled to 4° C for 30 minutes; of these, one was heated back to room temperature for 15–20 minutes (Fig. 1e, Fig. S1,2). The samples were then observed using light microscopy. As expected, for the sample containing sodium chloride, no significant change with temperature was observed, whereas the turbid sulphate and perchlorate samples contained droplets (Figure 1e). We verified that the observed structures were protein-enriched by centrifuging the samples, which resulted in two distinct phases: a transparent top phase and a turbid bottom phase. For both samples, UV measurements of the top phase indicated that they were depleted of protein and they did not show any features under the light microscope. There was a significant difference in the size of the droplets formed, in the order of 3.4 μm and 1 μm for sulphate and perchlorate, respectively (Figure 1f).

Anion-type and concentration determine the oligomerisation state

Having established the bulk properties of the insulin solution, and having identified anion-specific UCST-type behaviour, we wanted to gain a deeper understanding of the effects that the selected anions may have on the oligomerisation properties of insulin. To study this in the solution state, small-angle X-ray scattering was measured on freshly prepared insulin solutions (i.e., at time 0). Measurements were made at room temperature for a range of insulin and anion concentrations. Model-independent analysis was performed by plotting the data in the Kratky depiction and determining the radius of gyration from the Guinier plot. An example of the Kratky plot for a single anion (chloride, 100 mM) and two insulin concentrations is shown in Fig. 2a. Upon increasing insulin concentration whilst maintaining anion concentration, a shift in the Kratky plot maximum towards lower q values was observed, indicating an increase in the size of the protein under increasing insulin concentration. This insulin concentration-dependent increase in the size of the protein in solution was further verified by the radius of gyration (R_{g}) determined from the SAXS data; the gyration radii obtained are shown for all anions at two insulin concentrations in Fig. 2b. Although all conditions indicate an increase of R_{g} with increasing insulin concentration, both the value at the lowest insulin concentration and the extent of the observed increase were anion-dependent.

Insulin tends to form a range of oligomeric species (e.g., dimers, hexamers, Fig. 2c) in solution.[35] Thus, we questioned whether the changes in radius of gyration were due to the extent of oligomerisation. To test this hypothesis, we calculated theoretical scattering curves of different insulin oligomers from crystal structures and fitted them to SAXS data.[36] Good fits to the scattering data were obtained for most conditions, indicating that well-defined insulin oligomers were present in solution. For the neutral chloride anion, SAXS experiments and analysis were performed at three different anion concentrations at a fixed insulin concentration of 0.52 mM (Fig. 2d and Fig S4.). These results indicate that larger oligomeric species formed with increasing ionic strength from 100 to 500 mM. This is in

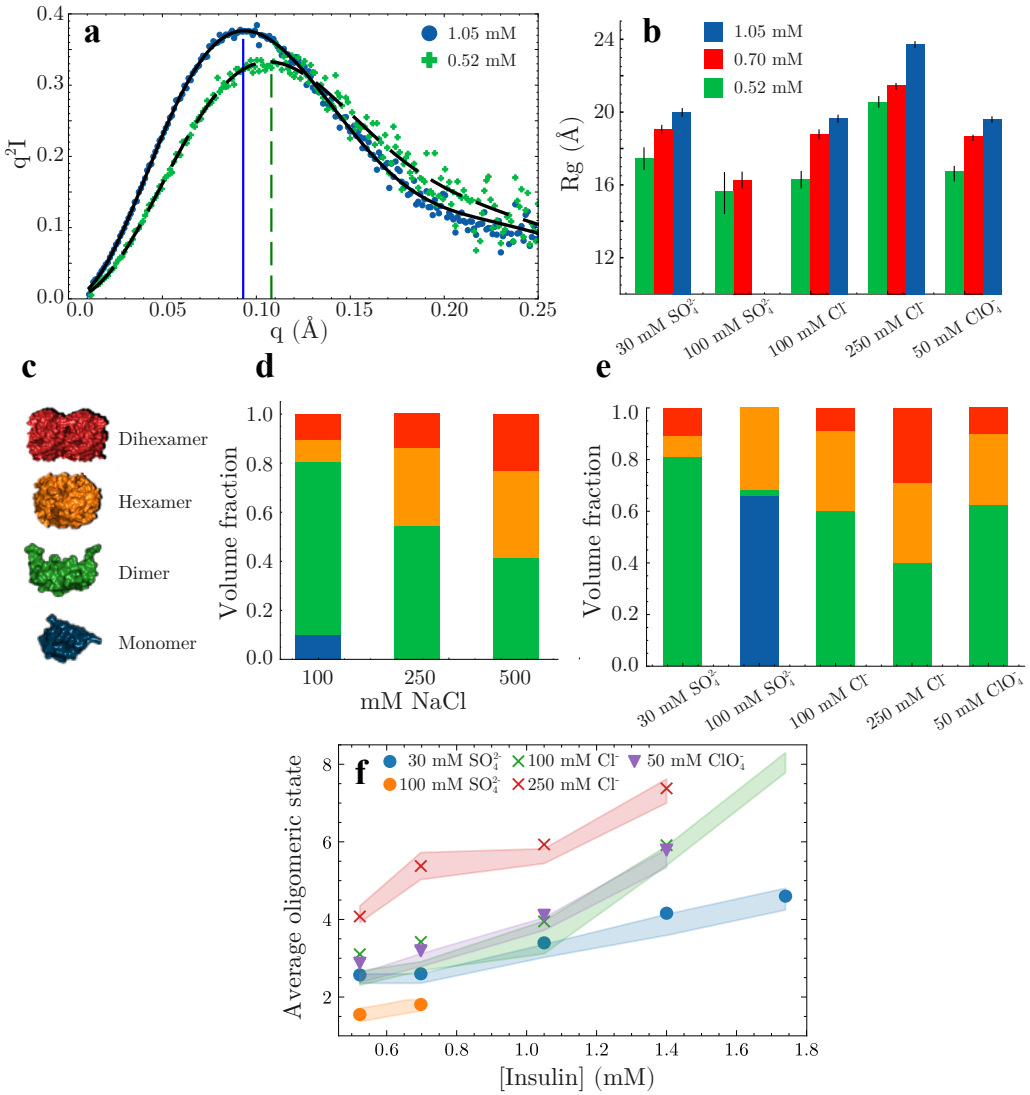

Figure 2: **(a)** SAXS data of insulin at the indicated concentration in 100 mM NaCl. The dashed line indicates the maxima, which shift to lower q with increasing insulin concentration. **(b)** Radius of the gyration of insulin samples under different ionic conditions at the indicated insulin concentration, determined from the Guinier fit to the SAXS data. **(c)** Depiction of insulin structures fitted to the SAXS data. **(d)** Distribution of oligomers determined from fitting of the SAXS data for 0.52 mM insulin at the indicated NaCl concentrations. The colours correspond to the oligomeric species shown in (c). **(e)** Distribution of oligomers determined from fitting the 4 mg/ml SAXS data shown to the indicated anion solutions; colours correspond to the oligomers shown in (c). **(f)** The average oligomeric state of insulin determined from the SAXS data based on the calculation of the oligomeric distribution (symbols) and the calculation of the volume directly from the SAXS data (shaded areas).

agreement with the expected increase in protein–protein interactions upon increasing the screening of charges in-solution. At the highest protein and anion concentrations measured, the fits obtained started to deviate from the experimental data because of the presence of oligomers or aggregates larger than those used to fit the data.

The average molecular mass was calculated from the theoretically obtained distribution of oligomeric species (Figs. 2e and f). To further verify that the oligomeric distribution obtained was accurate, the molecular mass was also calculated based on the volume calculated from the SAXS data (i.e., without fitting the insulin oligomeric structures) and compared with the molecular mass determined from the calculated oligomeric distribution (Fig. 2f). In general, a strong agreement was found between the two methods, supporting our conclusion that insulin oligomers were formed. Comparison at a single insulin concentration with varying anions (Fig. 2e) revealed that the chaotropic anion perchlorate resulted in similar distributions of oligomeric species compared to the intermediate Hofmeister-series chloride anion. However, the kosmotropic sulphate anion showed distinct effects. At 100 mM sulphate, a large fraction of monomeric insulin was present, which was not observed for any of the other anionic species or concentrations (Fig. 2e).

Based on observations from the the SAXS analysis, we conclude that, for all anions, there was insulin concentration-dependent oligomerisation, with more insulin participating in larger oligomers with increasing concentration. For the neutral chloride anion, a clear influence by the ionic strength on the extent of oligomerisation was observed, as expected of a purely electrostatic interaction. However, sulphate was an outlier, as a decrease in average molecular mass was observed with increasing sulphate concentration. Additionally, we observed that, at 100 mM sulphate, oligomerisation was inhibited and most of the insulin in-solution was present in the monomeric form.

Anions change the thermal stability of, and interact with, insulin in an anion-specific manner

To understand the specific ion effects of the selected anions and their interactions with insulin in more detail, we performed atomistic molecular dynamics (MD) simulations at 25° C and 65° C with varying concentrations of SO_4^{2-}, Cl^- and ClO_4^-. The stability of proteins is determined in part by the stability of the secondary structures present with the overall tertiary structure. Therefore, we determined the secondary structure propensity of each residue throughout the MD simulation according to temperature (25 or 65° C). These propensities were then subtracted from each other to yield the so-named delta secondary structure percentage (Figs. 3a, b and c), which depicts the change in secondary structure elements upon heating. For both chloride and perchlorate anion, a significant decrease in the alpha-helical nature of the first ten N-terminal residues was observed, while for sulphate, there was an increase in alpha-helical structure in this region. Between the C-terminal region of chain A and the N-terminal region of chain B, there was an increase in beta sheet-type structure in the presence of chloride. For perchlorate, there was no significant change in this region, although, for sulphate, there was a slight loss in random coil and an almost equal increase in alpha helix. The changes in the secondary structure upon heating can be summarised as follows: perchlorate demonstrated a loss of alpha-helical secondary structure in the N-terminal region and the same effect was observed for chloride coinciding with an increase in beta sheet. For sulphate, there was a slight increase in the alpha-helical structure in the N-terminal of both chains. For both perchlorate and sulphate, there was no detectable appearance of beta sheet upon heating.

The root-mean-squared fluctuations (RMSF) determined from the MD simulations are shown in Figs. 3d, e and f. At the start of chain B (i.e., residues 22-30), there was an increase in the RMSF for all three conditions. The fact that this region fluctuated more than the rest of the insulin protein is not surprising considering that this region is known to be flexible.[37] More significantly, this region fluctuated more heavily in the presence of the sulphate anion

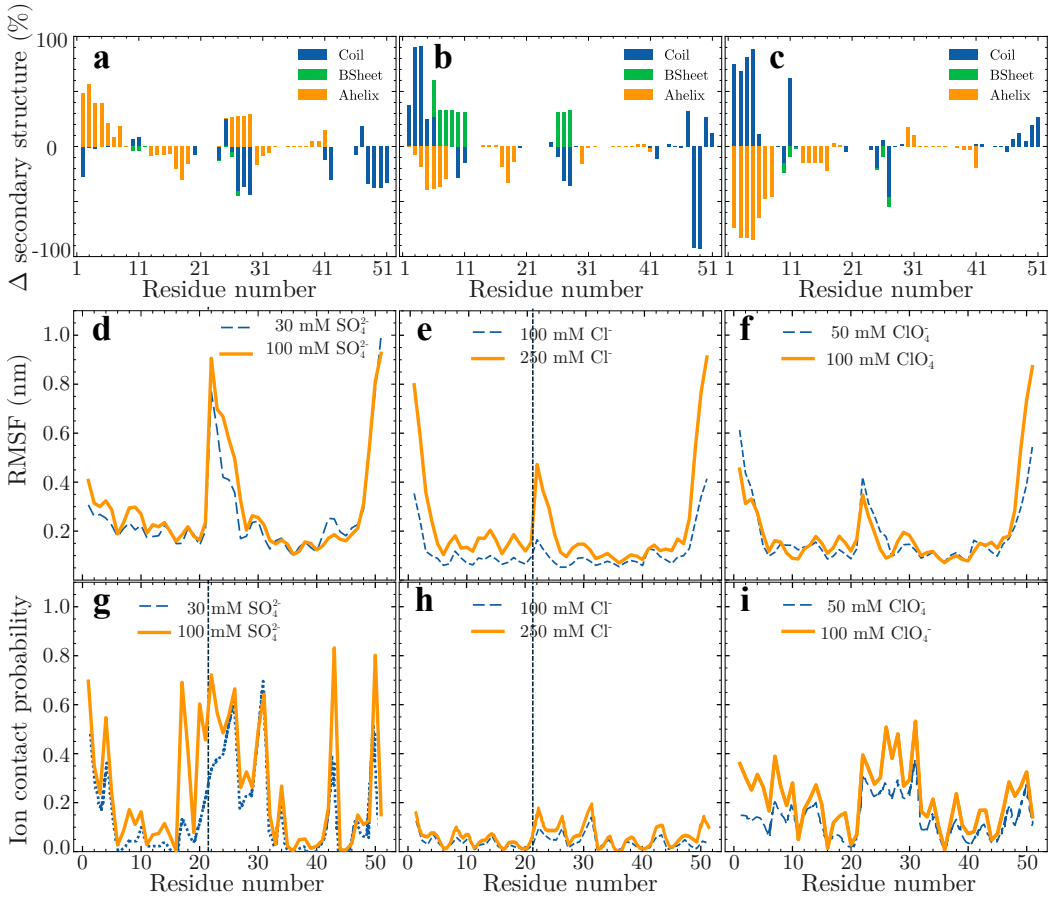

Figure 3: Results from the insulin MD simulations in the presence of the selected anions. **(a, b, c)** Change in insulin secondary structure observed upon heating to 65° C for (a) SO_4^{2-}, (b) Cl^-(c) ClO_4^-. **(d,e,f)** The root mean square fluctuations (RMSF) of Cα carbon atoms, at the ionic condition indicated in the legends, from the 25° C simulation. **(g, h, i)** Ion contact probability for each residue with anion and concentration indicated, from the 25° C simulations.

compared to in the presence of perchlorate and chloride anions. Increased fluctuations were also observed at the N-termini of chain A and the C-terminus of chain B, corresponding to unstructured flexible regions in the crystal structure of insulin (Figs. 3d, e and f).

To determine the extent to which specific ion-protein interactions differ between the selected Hofmeister anions, the ion contact probability on a per-residue basis was extracted from the MD simulations. For all anion conditions, there was no significant probability of ion contact between any of the insulin residues and the cation (Na^+). Similarly, the chloride anion did not show significant tendencies to interact with the insulin protein (Fig. 3h). On the contrary, for both perchlorate and sulphate, an increase in the probability of the ion interacting with insulin was observed at the C-terminal of chain A and at the N-terminal of chain B (Figs. 3g and f). This high anion contact probability, the highest for sulphate followed by perchlorate, and the lowest for chloride, coincided with a prolonged ion lifetime on the same residues with a high contact probability (Figs. S5, S6 and S7). Comparing the three anions, we can conclude that there was a ranking of anion interactions with the protein, in order of increasing interaction strength, of: chloride, perchlorate, and sulphate.

Hydrogen bonding underpins the strong anion-insulin interaction

From the MD simulations, the average number of hydrogen bonds per insulin residue at 25 and 65° C was extracted (Fig. 4a, b and c). The results show that sulphate formed several hydrogen bonds with insulin, while both perchlorate and chloride showed negligible hydrogen bond formation with insulin. On the basis of the apparent propensity for hydrogen bond formation between insulin and sulphate, we hypothesised that a combination of hydrogen bond formation and electrostatic interactions causes the tight interaction between sulphate and insulin. Compared with perchlorate, this tight interaction is increased because of the divalent negative charge and the presence of multiple hydrogen bond acceptors (the oxygens), allowing sulphate to form bidentate hydrogen bonds to adjacent proteins (Fig. 4d). The formation of at least two hydrogen bonds between the sulphate and adjacent insulin monomers

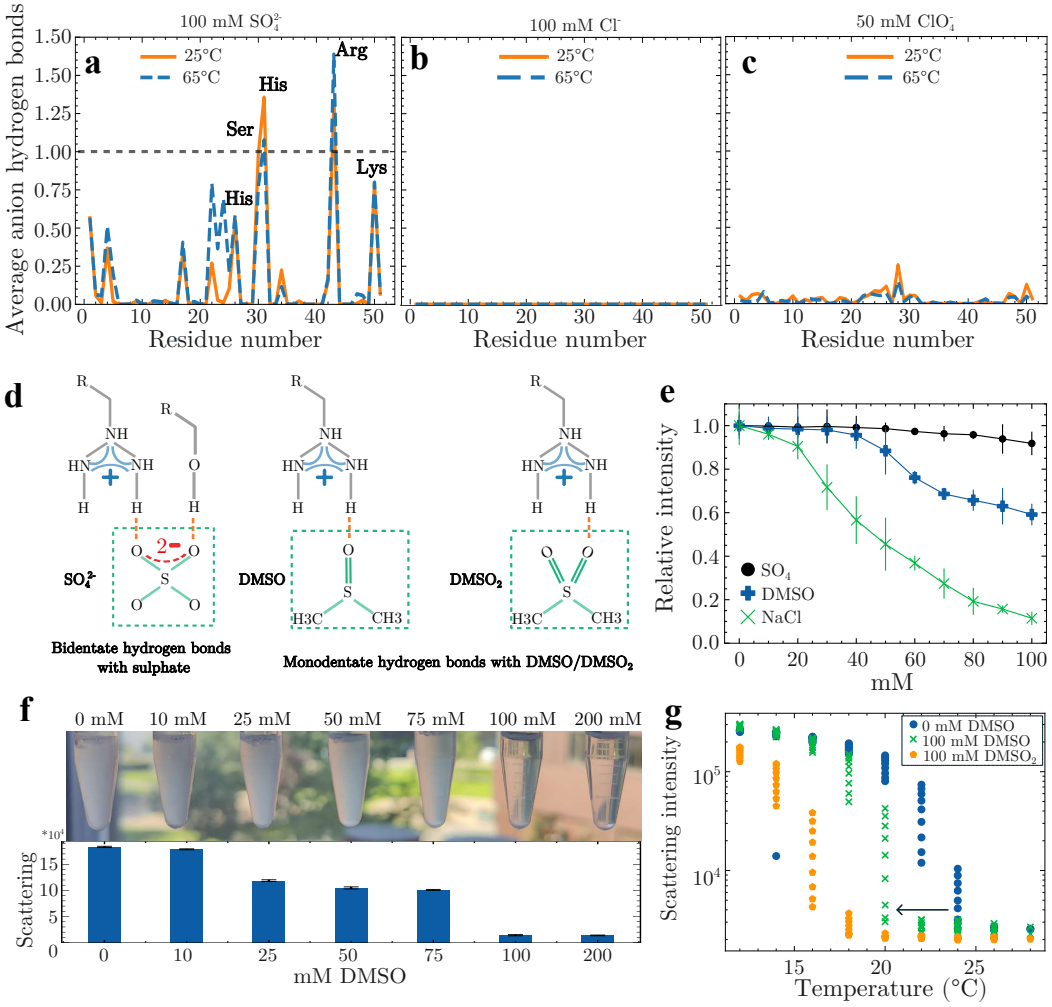

Figure 4: **(a, b and c)** Average number of hydrogen bonds between the residues of insulin and the indicated anions, extracted from the MD simulations. **(d)** Schematic depiction of potential hydrogen bond pairs between amino acid side chains and the indicated excipients **(e)** Effect of SO_4^{2-}, DMSO and NaCl concentration on the turbidity of an insulin sample in 100 mM SO_4^{2-} in the phase-separated state. **(f)** Top: Pictures of insulin solutions (0.6 mM) in 100 mM SO_4^{2-}, with increasing concentration of DMSO. The solutions were incubated at 8° C for 15 minutes. Bottom: Light scattering intensity measured for the corresponding samples shown in the top row. **(g)** Cloud point measurements performed for 600 μM insulin solutions containing 100 mM SO_4^{2-}, in addition to the indicated concentration of excipients. Measurements were performed by decreasing the temperature.

could act as a bridging interaction that results in the formation of a protein network. If present, this interaction could explain the enhanced propensity of sulphate to form droplets at a lower temperature.

To test the contribution of both electrostatic and hydrogen-bond interactions to the observed droplet formation, we titrated sodium chloride and DMSO into an insulin solution below the critical solution temperature whilst measuring the turbidity by scattering intensity. DMSO has been shown to act as a strong hydrogen bond accepting competitor, disrupting polymer networks formed by hydrogen bonding (Fig. 4d),[38] while the addition of sodium chloride increases the total ionic strength of the solution, thus increasing the Debye length and increasing the screening of potential electrostatic interactions. Titration experiments were also performed with sulphate to account for any potential intrinsic dilution effects in the experiment.

The results of the titration experiment are shown in Fig. 4e. Upon titration of sulphate into the turbid insulin solution, only a small decrease of intensity was observed, indicating that turbidity persisted upon slight dilution during the experiment. Titration of both DMSO and sodium chloride resulted in a dramatic decrease in the measured turbidity, with sodium chloride having a stronger effect than DMSO. These data indicate that it is a combination of electrostatics and hydrogen bonding that contributes to the interactions that stabilise the observed droplets. Having tested how DMSO influences the droplets of already formed solutions, we next prepared fresh insulin solutions at a fixed concentration (0.6 mM) above the critical temperature, containing increasing concentrations of DMSO. These solutions were then cooled below the critical temperature for 15 minutes. As expected, a decrease in turbidity was observed with increasing DMSO concentration (Fig. 4f), with 100 mM DMSO producing completely clear solutions. This result contrasts with the data shown in Fig. 4e, where turbidity persisted at 100 mM DMSO. This can be explained by the two different experimental protocols used. Indeed, in Fig. 4e, DMSO was added to solutions already containing droplets (i.e., ion–insulin H-bonds already formed) while, in Fig. 4f, DMSO was

added prior to hydrogen bond formation and formation of the dense phase.

In a final experiment, we wanted to monitor the impact of H-bonds on the cloud point of insulin, so we performed the experiment on insulin solutions in the presence of 1) 100 mM sulphate, 2) 100 mM sulphate and 100 mM DMSO, and 3) 100 mM sulphate and 100 mM $DMSO_2$. Compared to DMSO, $DMSO_2$ contains an additional oxygen available for the H-bond (Fig. 4d). Although cloud point temperatures of 24 and 20° C were detected for sulfate and DMSO, respectively, in the presence of $DMSO_2$, this value further decreased to 16° C, showing a crucial effect of the ion-protein H-bonds in determining the formation of the insulin dense phase.

In summary, the interaction between sulphate and insulin is caused by a combination of electrostatic interactions and hydrogen bonding. Reducing the contribution of these interactions resulted in a decrease in the droplet phase. The formation of the droplet phase is caused by the ability of both perchlorate and sulphate to form bidentate hydrogen bonds, resulting in the crosslinking of a large number of insulin monomers. However, compared to perchlorate, sulphate solutions exhibited a higher critical temperature and formed larger droplets. This can be explained by the divalent charge of sulphate, which enhances the hydrogen bond formation with the protein, resulting in tighter anion binding and the formation of larger protein networks.

Anions determine aggregation kinetics and amyloid morphology

The aggregation kinetics of insulin at 65°C in the presence of the three Hofmeister anions are shown in Fig. 4a. Compared to both perchlorate and chloride, sulphate displayed a slower growth rate that coincided with a prolonged period of time to reach the plateau phase. The overall kinetic profile observed for sulphate differed significantly from the sigmoidal pathway observed for classical amyloid fibrils (Fig. 4a).[39,40] The prolonged delay time and reduced kinetics were consistent with previous experimental data, showing that, with sulphate, large aggregates without beta-sheets were initially formed, which converted over time to ThT-

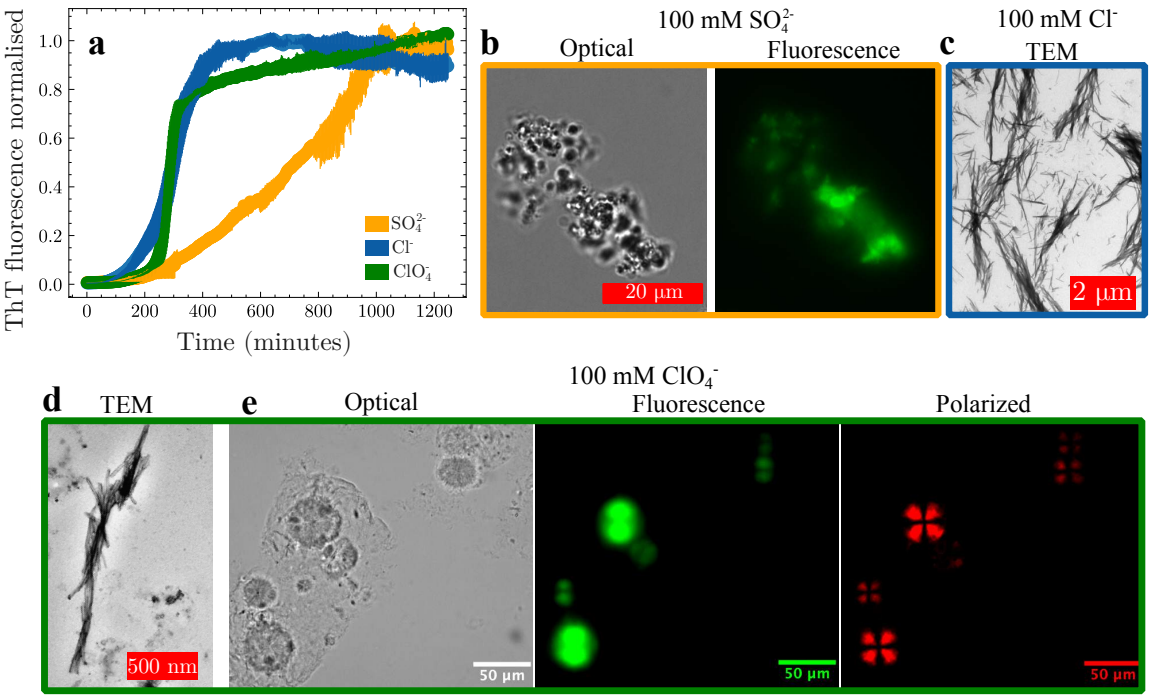

Figure 5: **(a)** Aggregation kinetics of 600 μM insulin at pH 2 and 65°C in the presence of 100 mM of the indicated anion, measured by ThT fluorescence. **(b)** Amyloid particulates formed in 100 mM SO_4^{2-} and stained by Thioflavin-T, as observed through optical and fluorescence microscopy. **(c)** TEM of amyloid fibrils observed in 100 mM Cl. **(d)** TEM of amyloid fibrils observed in 100 mM ClO_4^-. **(e)** Optical microscopy, ThT fluorescence, and polarised light microscopy of insulin in 100 mM ClO_4^-, stained with Thioflavin T. The polarised light microscopy images reveal a Maltese cross pattern characteristic of spherulitic amyloid aggregates.

positive beta-sheet aggregates.[32,39] The formation of microparticles named particulates is evident in the microscopy images (Fig. 4b) taken at the end of the aggregation process, showing ThT-positive, sphere-like structures without any birefringence, and is in agreement with our previous work.[33] Sodium chloride resulted in sigmoidal aggregation kinetics with a lag phase followed by rapid growth, resulting in the formation of ThT-positive amyloid fibrils (Fig. 4C). Compared to chloride, perchlorate caused a slight increase in the initial lag phase, followed by a rapid growth phase, resulting in the formation of predominantly spherulite structures, characterised by a Maltese-cross pattern under polarised light, with some amyloid fibrils (Figs. 4d and e).

Discussion

Proteins may self-assemble into various forms of amyloids, from elongated fibrillar structures and dense spheres, called particulates, to hedgehog morphologies called spherulites, resembling a structure commonly encountered in polymer science.[33,39,41] These structures have been observed both in vivo and in vitro, and are considered general pathways for a number of proteins, independent of their amino acid sequence.[42–44] Electrostatic interactions between proteins are the major determinant of this heterogeneity of amyloid structures, but the precise mechanism that leads to this diversity is still unknown. In this work, we used a selection of Hofmeister anions below concentrations where one would expect to see the kosmotropic and chaotropic nature of Hofmeister anions (typically above 300 mM). Despite the low concentrations used, the selected Hofmeister anions regulated the formation of distinct amyloid morphologies (Fig. 5).[33]

To determine how these different anions exert such a drastic influence on the observed aggregation phenomena, we first studied their effects on the solution properties of insulin prior to aggregation. We observed that, in the presence of both sulphate and perchlorate, but not chloride, insulin solutions displayed an upper critical solution temperature, below which formed droplets are enriched with protein (Fig. 1). Compared to perchlorate, sulphate had

a higher critical solution temperature and, at the same temperature, formed larger protein droplets and thus had a stronger effect on the solution properties of insulin.

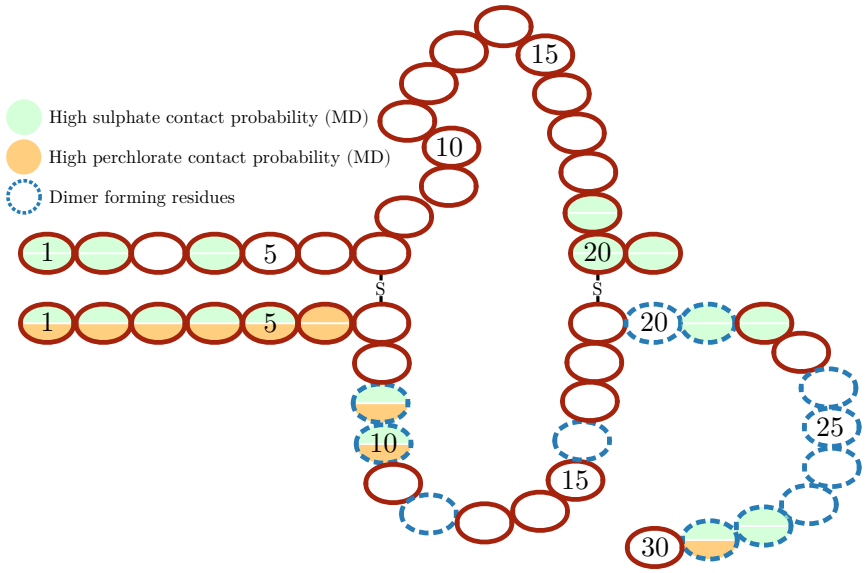

Figure 6: The primary structure of insulin depicting the A- and B-chain linked together by disulphide bonds. Residues with an ion contact probability determined by the MD simulation to be more then 0.4 are highlighted for perchlorate and sulphate.

On the macroscopic scale, data from the MD simulations showed that heating both perchlorate and chloride caused a decrease in the alpha-helical content of insulin and the presence of chloride even induced the formation of beta sheets (Fig. 3). On the other hand, in the case of sulphate, there was only a slight increase of alpha helix upon heating and an absence of beta sheet formation. This observation corroborates previous experimental data, which showed that sulphate can lock in the insulin monomer state with an enhanced conformational stability against temperature increases.[32] Further examination of the MD data showed that the interactions between the anions and insulin followed a ranking of, in order of increasing interaction strength: chloride, perchlorate and sulphate. For the monovalent and monoatomic anion chloride, no specific ion contact probability was observed with insulin and, unsurprisingly, no specific hydrogen bonds formed (Fig. 3). For perchlorate, which has the same charge as chloride and a similar ionic radius,[45] but which does have the ability to act as a hydrogen bond acceptor, an increase in the ion contact probability with

insulin was predominantly found at the first 6 N-terminal residues of the B-Chain (Fig. 6). For sulphate, an even higher contact probability was observed, coinciding with both a prolonged life-time of ion contact and a high degree of hydrogen bond formation. Similarly to perchlorate, sulphate also interacted highly with the N-terminal of the B-chain, as well with the dimer-forming region of the B-chain and the N-terminal of the A-chain (Fig. 6). We thus questioned whether this increased ability of sulphate to bind to insulin was due to the formation of hydrogen bonds with the protein, as suggested by the MD data, and whether this could explain the observed protein condensation at low temperatures and increased stability at higher temperatures. Experimental evidence from titration experiments with DMSO and sodium chloride showed that both hydrogen bonds and electrostatic interactions are important for the observed droplet formation (Fig. 4). This also explains why, for perchlorate, UCST behaviour was observed but not as strongly as for sulphate, because the latter is divalently charged, allowing for the strong formation of multiple hydrogen bonds that form the protein network within the droplet.

Previously, the crystal structure of insulin was determined under similar conditions, specifically at pH 1.7 in the presence of sulphate.[46] When our sulphate-containing samples were left at room temperature, we also observed the formation of protein crystals after 48 hours (Fig. 7 and Fig. S3). The previously determined crystal structure also showed the binding of several sulphate molecules to the protein, and several of those regions agree with the data from our MD study (Fig. 6). In the crystal structure, the sulphates also bridge adjacent insulin monomers in the crystal, highlighting the ability of sulphate to act as a crosslinker.

Having established that the hydrogen bonding of sulphate enhanced by electrostatic interactions influences both the phase behaviour and crystallisation of insulin, we next compared the solution properties of insulin at room temperature at time 0. For all anions, we observed both anion- and concentration-dependent increases in the average size of the insulin solutions. By fitting crystal structures of different oligomeric states of insulin, we showed that

this was due to changes in the extent of oligomerisation (Fig. 2). In general, larger oligomers were formed with increasing concentration. However, for sulphate, we observed a distinct lack of oligomers even at higher protein concentrations, and the predominant species present was instead monomer. We propose that this effect may also be caused by the tight binding of sulphate, specifically to the dimer-forming region which prevents further oligomer formation (Fig. 6). In the case of the crystal formation, it was suggested that this specific binding of sulphate to insulin acts to neutralise the surface charge of the protein, thus propagating the crystallisation process.

Previous experimental studies of lysozyme have observed a similar effect. Gokarn et al. measured the charge of lysozyme at relatively low ionic concentrations, such as below 100 mM.[47] They observed a decrease in the effective charge of lysozyme following the order: chloride, perchlorate, sulphate. They attributed this decrease in effective surface charge to increases in specific binding of sulphate compared to the other anions.

In order to understand how the specific interactions of the anions influence the final morphology of amyloids formed, we performed a range of microscopy experiments. Based on the results in Fig. 5 and previous experimental data, the influence of the anions on the final amyloid morphology is as follows: sulphate results in mainly amyloid-like spherical microparticles (particulates), chloride produces mainly amyloid elongated fibrils, and perchlorate produces a mixture of fibrils and spherulites.[33]

If we consider a homogeneous solution of insulin away from the PI, the proteins in solution are positively or negatively charged, and long-range electrostatic repulsion between monomers stabilises the solution. However, if there is specific ion binding to the surface of the protein, the net charge is reduced, allowing neighbouring proteins to approach it more closely. This is the case for sulphate anion, which interacts strongly through a combined hydrogen and electrostatic interactions. At low temperatures, this results in the critical solution temperature previously mentioned. As the temperature is increased, the tendency for proteins to aggregate increases. Importantly, in the case of sulphate, ion binding also

enhances the conformation stability of the protein (Fig. 3). In this configuration, it should be expected that the aggregation process will exhibit features similar to a coalescence of colloidal particles, with the protein initially maintaining its structural arrangement and approaching neighbouring protein molecules. Indeed, our ThT fluorescence data (Fig. 5) show that the formation of structures rich in beta sheet proceeded more slowly in the presence of sulphate compared to either perchlorate or chloride. This result is in line with the work of Owczars and Arosio, who showed that, under conditions similar to those studied here, the lag time of insulin aggregation approximately doubled when the anion was changed from chloride to sulphate (i.e., 2.5 vs 5 hours).[32] In the same study, solutions of insulin and sulphate showed a dramatic increase in hydrodynamic radius prior to the onset of beta sheet formation. This means that, already in the early phase of the process, larger aggregates are formed, which retained their alpha helical structure for a prolonged period before undergoing a beta-sheet transition.

This process can be explained by the presence of a locked monomeric state of insulin and reduced electrostatic repulsion, induced by the tight binding of sulphate to the surface. Together, these two aspects result in a colloidal-like aggregation reaction in which structurally unchanged proteins coalesce and form spherical particles. This pathway, termed the colloidal pathway, is depicted schematically in Fig. 7. The microparticles formed by coalescence eventually undergo beta-sheet transition at later stages, as previously observed for both insulin and alpha-lactalbumin.[32,39] We propose that the tight binding of sulphate to insulin, due to a combination of hydrogen bonding and electrostatic interactions and resulting in a reduced net charge and an enhanced conformational stability, is at the basis of both the appearance of the protein-dense phase at low temperatures and the formation of amyloid particulates at high temperatures.

Under aggregation conditions and in the presence of chloride anions, we mainly observed the formation of amyloid fibrils. Previous work reported a full correlation between scattering and ThT kinetics, suggesting that the massive aggregation observed in chloride solutions is

paralleled with an alpha helix-to-beta sheet transition.[48] We term this traditional pathway the conformational pathway (Fig. 7).

Finally, in the case of perchlorate, the reality lies somewhere between the other two. Compared to chloride, perchlorate binds more tightly to insulin, with slight hydrogen bond formation, but not as strongly as sulphate, resulting in a weaker UCST-type behaviour (Fig. 1). Upon aggregation of insulin in perchlorate solutions, a more complex scenario emerges, and both amyloid fibrils and spherulites are observed. The latter are described as a core-shell structure, characterised by a radially growing beta-sheet aggregates on a disordered precursor core.[49,50] This apparent heterogeneity of amyloid morphologies can be explained by interplay between a purely colloidal pathway and a conformation-driven reaction. Indeed, at higher temperatures, the electrostatic repulsion between insulin monomers is still reduced, but not to the same extent as for sulphate anions. This fact allows for the formation of smaller aggregates by coalescence. However, the conformational stability of the insulin-perchlorate system is also reduced compared to the sulphate sample (Fig. 3), allowing a higher propensity towards conformational changes. At high temperatures, this last aspect has two main consequences. In one case, unfolded proteins undergo a purely conformation-driven reaction, similar to the case of the insulin–chloride aggregation and resulting in the formation of amyloid fibrils. As a second pathway, the aggregates formed by coalescence act as a nucleation site for unfolded proteins, which, in turn, promotes the formation of radially growing aggregates, eventually defining the fingerprint of spherulites (Fig. 7).

In summary, we demonstrate that the specific interactions of anions from the Hofmeister series regulate not only the phase behaviour and stability of insulin but also the solid transitions to crystalline and amyloid forms. We report that the interactions responsible for the droplet formation of insulin at low temperatures are the determinants of the solid transition at higher temperatures, both in terms of crystals (at room temperature) and amyloid aggregates at higher temperatures. In the latter case, the interactions regulating the dense

phase are also responsible for the balance between colloidal and conformational stability of the protein, leading to diverse pathways and a pronounced heterogeneity in the structure and morphology of the amyloid aggregates.

In the context of neurodegenerative diseases, the aggregate polymorphism is associated with different patterns of neuropathology,[51,52] while the adverse biological effects of protein drugs depend on the structure of the aggregate.[53–55] Our findings address the concept of morphological fingerprint of aggregates encoded in the LLPS propensity of a protein. This perspective may guide a more tailored screening of modulators for protein aggregation, especially if specific amyloid polymorphs are targeted. The identification of protein condensed phases will indeed serve as a rapid prediction method for potential aggregate structures and conformations. In addition, short-lived intermediate species and oligomers are indicated as targets for pharmacological treatments, but their isolation is often challenging, even in in vitro experiments.[56] In this regard, protein-dense phases will provide a more accessible and long-lived protein ensembles for testing molecules that can inhibit or reverse the aggregation process, paving the way for novel opportunities in the treatment of degenerative disorders and protein drug development.

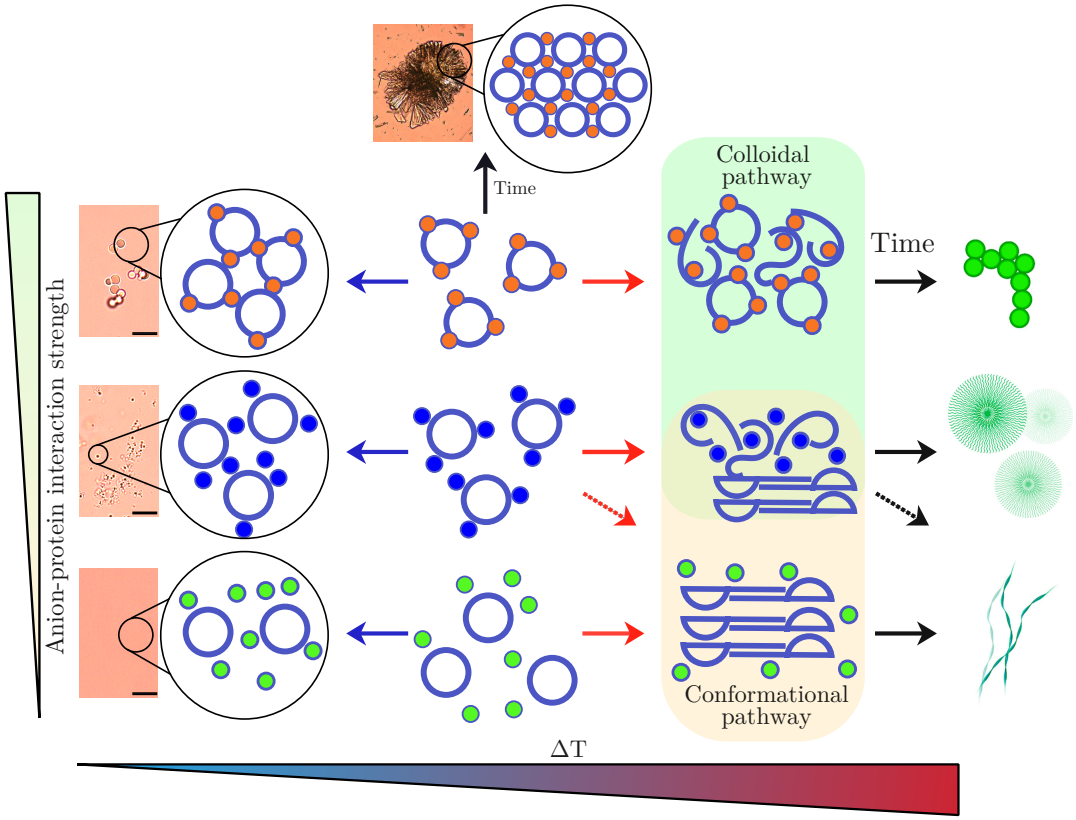

Figure 7: **Schematic overview of the results. Top row:** Colloidal pathway imposed by sulphate ions that interact specifically with insulin resulting in a reduction of the net positive surface charge. Upon heating, larger aggregates are formed that retain the folded structure. Over time, these aggregates convert to the beta-rich structures observed in amyloids. Attractive inter-protein interactions can also be observed when the mixture is cooled, resulting in phase separation, and when left at room temperature, causing the formation of protein crystals. **Middle row** Perchlorate results in an intermediate between the colloidal and conformational pathways. There is reduced UCST behaviour, and no protein crystals are observed after incubation at room temperature. Aggregates form but grow predominantly through the recruitment of unfolded monomers, resulting in the formation of predominantly spherulite structures. **Bottom row** Conformational pathway imposed by chloride anions. The chloride anions do not interact specifically with the protein and instead provide charge screening based on ionic strength. The formation of amyloid is driven by the unfolding of the insulin protein, resulting in the formation of beta sheet-rich elongated fibrils.

Methods

Chemicals

Human insulin (91077C, 95%), sulphate (99%), sodium chloride (99%), sodium, sodium perchlorate (98%) were purchased from Sigma-Aldrich, Germany. Sodium hydroxide (99%) and hydrochloric acid (99%) were purchased from Merck, GermanyTh.Geyer and CHEM-SOLUTE, Denmark, repsectively.

Solubility measurements

Fresh samples of insulin were prepared by dissolving a known amount of insulin and setting the pH to 2.0 by titration of HCl. The samples were then filtered through a 0.22 μm syringe filter (Labsolute, Th.Geyer, Germany) and the final concentration of insulin was determined by triplicate measurements of U.V. absorbance with a Nanodrop system (Thermo Fisher). The freshly prepared samples of insulin were then placed in a quartz cuvette with a stirring bar and incubated at the specified temperature in a Labbot instrument (ProbationLabs, Sweden). The autotitration system of the instrument was used to slowly titrate 1 M of either sulphate, perchlorate or chloride into the insulin sample, whilst simultaneously measuring the scattering at 90 degrees and the U.V. absorbance in the range 280-600 nm. The data were plotted as a function of salt concentration, after correcting for the dilution effect due to the titration. The concentrations at which a jump in the scattering at 90 °(or the absorbance at high wavelengths) took place was determined to be the solubility limit. Each measurement was repeated at least 3 times.

Temperature dependence measurements – single-angle light scattering experiments

Fresh insulin samples were prepared as before at pH 2, in 100 mM sodium sulphate, perchlorate or chloride. After filtering, the samples were placed in a quartz cuvette with a

stirring bar in the Labbot instrument and allowed to equilibrate for at least 30 minutes at 12 degrees. During the experiment the stirring was turned on and the temperature ramped by 2 degrees every 3 minutes. During the temperature run the scattering intensity of a 636 nm laser at 90˚angle was measured. The scattering was then normalised by the lowest measured scattering intensity for each sample.

Titration measurements – single-angle light scattering experiments

Fresh insulin samples were prepared as before at pH 2, in 100 mM sulphate. After filtering, the samples were placed in a quartz cuvette with a stirring bar in the Labbot instrument and allowed to equilibrate for at least 30 minutes at 12°C. During the experiment the stirring was turned on. Every 5 minutes ten microlitres of 1M NaCl, 1M DMSO or 1M Na_2SO_4 was titrated into the solution, after which the light scattering intensity was measured at 90°.

Microscopy measurements

For the detection of the protein rich droplets, samples were prepared by dissolving the insulin in the desired anion concentration and setting the pH to 2.0. After preparation the samples were filtered through a syringe filter (0.22 μm) and the insulin concentration was confirmed by triplicate measurements of the U.V. absorbance at 280 nm. The samples were then left to equilibrate at 4°C for at least 30 minutes before imaging. One of the samples was, however, first heated back to room temperature for a period of about 30 minutes before imaging. 15-30 μl of the samples were then placed on a glass slide and covered with a 22x26 mm cover slip and directly imaged with a 64x oil objective (Zeiss, Germany) using a Leica DMi8 optical microscope (Leica Microsystem, Wetzlar, Germany) using either brightfield, fluorescence (excitation 488 nm and emission at 530 nm) or polarized light settings. The morphology of the protein aggregates (spherulites and particulates) and crystals was detected by using a DMi8 optical microscope (light microscope, LM) with a 10x, 20x and a 63x oil objective (Leica Microsystem, Germany). 10-15 μl of the aggregates/crystals were placed on a glass

slide prior to imaging and analyzed in polarized, brightfield and fluorescence modes.

Data Collection Small-angle X-ray scattering (SAXS)

5 mg of HI powder was dissolved in 1 mL of 30 and 100 mM sodium sulphate, 100; 250 and 500 mM sodium chloride; and 50 and 100 mM perchlorate. Sodium hydroxide and hydrochloric acid were used to adjust the pH to 2.00 $\pm$ 0.05. Afterwards, the samples were filtered through a 0.22 μm cellulose filter (Labsolute, Th.Geyer, Germany) and the final concentration of insulin determined by U.V. absorption at 280 nm. 20-30 μl of each sample was transferred to a 96-well plate. The SAXS studies were performed at the CPHSAXS Facility, University of Copenhagen, using a BioXolver L (Xenocs) with a wavelength of $\lambda = 1.34$ Å. Primary data reduction was made in BIOXTAS RAW.[57] Experiments were conducted at room temperature, with samples prepared immediately before the experiment and then stored on ice until loading the sample. Scattering from the corresponding buffers was measured under identical conditions (i.e. same exposure time) and subtracted from the sample scattering.

Data analysis – SAXS

For each solution condition the radius of gyration was determined by linear fitting to the Guinier region (Ln(I) against q^2) that satisfied $q \cdot Rg <= 1.3$. The SAXS data were fitted using the program OLIGOMER from the ATSAS package[58] , using the crystal structures of insulin and insulin oligomers taken from the PDB (PDB ID: 3i40,1guj,1ai0).[46,59,60] From the distribution of oligomers the average molecular mass was calculated. The Mw was further calculated from each scattering curve using the DatBayes method implemented in PrimusQT from the ATSAS package.[58,61]

Aggregation kinetics monitored by ThT fluorescence

A stock solution of 1 mM ThT was prepared by dissolving ThT in milli-Q water and filtering through a 22 μm syringe filter (Labsolute, Th.Geyer, Germany). ThT was added to the solutions containing insulin at 600 μM and a 100 mM $NaCl/Na_2SO_4/NaClO_4$, to a final concentration of 20 μM. 200 μL of each protein solution was transferred to a 96-well plate (NUNC, Thermo Fisher, USA). ThT fluorescence was measured on a CLARIOstar (BMG Labtech, Germany) plate reader using 450 nm for excitation and a 490 nm filter for detection using the bottom optics. At least 4 repetitions were made for each sample.

Transmission Electron Microscopy (TEM)

The morphology of the fibrils was observed by TEM using a Philips CM 100 TEM (Philips, The Netherlands) operated at voltage of 80 kV. Images were recorded with the ITEM software package. 5 μl of the sample were negatively stained and mounted on hydrophilic grids (by glow discharge) prior to imaging.[62]

Molecular dynamics (MD) simulations

The initial structure of HI was obtained from PDBs 2mvc.[63] To mimic the experimental pH 2 level conditions, protonated Lys, Glu, and His were used for modelling the insulin. Also, charged N- and C- termini were used ($NH3^+$, COO^-). The insulin carried an overall charge of +5. The HI was placed in a cubic box of 400, 280 nm^3, with 1.5 nm from the box walls. Each system was solvated by TIP3P water models, then different Hofmeister salt (sodium chloride, sodium sulphate and sodium perchlorate) concentrations were added to mimic the experimental conditions and neutralize the systems. The All-atom MDs were performed using GROMACS 2020 simulation package[64,65] with Amber14SB forcefield[66] and the parameters of the ion developed by Kashefolgheta and Baaden for sulphate and perchlorate, respectively.[67,68] The systems were first energy minimized using the steepest descent minimization algorithm to remove any local atomic clashes.[69,70] Subsequently, the systems

were equilibrated under an isothermal–isobaric NPT ensemble for 100 ps, where the desired temperatures (25 or 65°C) were achieved using a velocity-rescale thermostat method with a coupling time constant of 0.1 ps.[71] While the pressure was kept at 1 Pa using the Parrinello-Rahman pressure coupling method with a coupling time constant of 1.0 ps.[72–74] During the equilibration process, a position restraint with a force constant of 1000 kJ/mol.nm^2 for protein heavy atoms was applied. The production runs followed, which were performed under NPT ensemble using Nose-Hoover[75–78] thermostat and a Parrinello–Rahman barostat with a relaxation time of 2 ps. The particle mesh Ewald method (PME) was used to compute the electrostatic interactions.[79,80] The cutoff distances of van der Waals and Coulomb forces are set to 1.2 nm in real space under the periodicity assumptions; periodic boundary conditions set in all directions were utilized. All bonds were restrained using the LINCS algorithm. For the production runs, each system was initially simulated for 1 μs, from which two structures selected from the clustering analysis were used as starting structures for the next 2 $\times$ 1 μs simulations.

Acknowledgement

V.F., S.J.L. and H.C. acknowledge VILLUM FONDEN (Villum Young Investigator Grant "Protein Superstructures as Smart Biomaterials, ProSmart", Grant 19175) and the Novo Nordisk Foundation (NNF20OC0065260) for funding the project. The authors acknowledge the Core Facility for Integrated Microscopy, Faculty of Health and Medical Sciences, University of Copenhagen. The authors thank the VILLUM FONDEN (Grant 19175) for funding the CLARIOstar plate reader and VILLUM FONDEN (Grant 19175), the Novo Nordisk Foundation (Grant NNF16OC0021948) and the Lundbeck Foundation (Grant R155-2013-14113) for funding the Leica DMi8 microscope. The authors gratefully acknowledge computing time on the supercomputer JURECA at Forschungszentrum Jülich under grant name AMYSALT. M.K. and B.S. are grateful for funding from the Palestinian–German Science

Bridge financed by the German Federal Ministry of Education and Research (BMBF).

Supporting Information Available

Further microscopy, SAXS and MD data are included in the Supporting Information.

References

(1) Ray, S.; Singh, N.; Kumar, R.; Patel, K.; Pandey, S.; Datta, D.; Mahato, J.; Panigrahi, R.; Navalkar, A.; Mehra, S.; others alpha-Synuclein aggregation nucleates through liquid–liquid phase separation. *Nature Chemistry* **2020**, *12*, 705–716.

(2) Murthy, A. C.; Dignon, G. L.; Kan, Y.; Zerze, G. H.; Parekh, S. H.; Mittal, J.; Fawzi, N. L. Molecular interactions underlying liquid- liquid phase separation of the FUS low-complexity domain. *Nature Structural & Molecular Biology* **2019**, *26*, 637–648.

(3) Gui, X.; Luo, F.; Li, Y.; Zhou, H.; Qin, Z.; Liu, Z.; Gu, J.; Xie, M.; Zhao, K.; Dai, B.; others Structural basis for reversible amyloids of hnRNPA1 elucidates their role in stress granule assembly. *Nature communications* **2019**, *10*, 2006.

(4) Kanaan, N. M.; Hamel, C.; Grabinski, T.; Combs, B. Liquid–liquid phase separation induces pathogenic tau conformations in vitro. *Nature communications* **2020**, *11*, 2809.

(5) Boeynaems, S.; Alberti, S.; Fawzi, N. L.; Mittag, T.; Polymenidou, M.; Rousseau, F.; Schymkowitz, J.; Shorter, J.; Wolozin, B.; Van Den Bosch, L.; others Protein phase separation: a new phase in cell biology. *Trends in Cell Biology* **2018**, *28*, 420–435.

(6) Babinchak, W. M.; Surewicz, W. K. Liquid–liquid phase separation and its mechanistic role in pathological protein aggregation. *Journal of molecular biology* **2020**, *432*, 1910–1925.

(7) Ahmad, A.; Uversky, V. N.; Khan, R. H. Aberrant liquid–liquid phase separation and amyloid aggregation of proteins related to neurodegenerative diseases. *International Journal of Biological Macromolecules* **2022**, *220*, 703–720.

(8) ten Wolde, P. R.; Frenkel, D. Enhancement of protein crystal nucleation by critical density fluctuations. *Science* **1997**, *277*, 1975–1978.

(9) Condensation, P. Kinetic Pathways to Crystallization and Disease, ed. JD Gunton, A. Shiryayev and DL Pagan. 2007.

(10) Vekilov, P. G. Dense liquid precursor for the nucleation of ordered solid phases from solution. *Crystal Growth & Design* **2004**, *4*, 671–685.

(11) Vekilov, P. G. The two-step mechanism of nucleation of crystals in solution. *Nanoscale* **2010**, *2*, 2346–2357.

(12) Gibbs, J. W. On the equilibrium of heterogeneous substances. **1879**,

(13) Volmer, M.; Weber, A. Keimbildung in übersättigten Gebilden. *Zeitschrift für physikalische Chemie* **1926**, *119*, 277–301.

(14) Xu, S.; Zhang, H.; Qiao, B.; Wang, Y. Review of liquid–liquid phase separation in crystallization: From fundamentals to application. *Crystal Growth & Design* **2021**, *21*, 7306–7325.

(15) Yuan, C.; Yang, M.; Ren, X.; Zou, Q.; Yan, X. Porphyrin/Ionic–Liquid Co-assembly Polymorphism Controlled by Liquid–Liquid Phase Separation. *Angewandte Chemie* **2020**, *132*, 17609–17613.

(16) Nyström, G.; Mezzenga, R. Liquid crystalline filamentous biological colloids: Analogies and differences. *Current Opinion in Colloid & Interface Science* **2018**, *38*, 30–44.

(17) Woods, J. M.; Nesta, D. Formulation effects on opalescence of a high-concentration MAb. *BioProcess Int* **2010**, *8*, 48–59.

(18) Samlaska, C.; Reber, S.; Murry, T. Insulin-derived amyloidosis: The insulin ball, amyloidoma. *JAAD Case Reports* **2020**, *6*, 351–353.

(19) Nagase, T.; Katsura, Y.; Iwaki, Y.; Nemoto, K.; Sekine, H.; Miwa, K.; Oh-i, T.; Kou, K.; Iwaya, K.; Noritake, M.; others The insulin ball. *The Lancet* **2009**, *373*, 184.

(20) Zhang, Z.; Huang, G.; Song, Z.; Gatch, A. J.; Ding, F. Amyloid Aggregation and Liquid–Liquid Phase Separation from the Perspective of Phase Transitions. *The Journal of Physical Chemistry B* **2023**, *127*, 6241–6250.

(21) Huang, S.; Xu, B.; Liu, Y. Calcium promotes α-synuclein liquid-liquid phase separation to accelerate amyloid aggregation. *Biochemical and biophysical research communications* **2022**, *603*, 13–20.

(22) Buell, A. K.; Hung, P.; Salvatella, X.; Welland, M. E.; Dobson, C. M.; Knowles, T. P. Electrostatic effects in filamentous protein aggregation. *Biophysical journal* **2013**, *104*, 1116–1126.

(23) Lenton, S.; Hervø-Hansen, S.; Popov, A. M.; Tully, M. D.; Lund, M.; Skepo, M. Impact of arginine–phosphate interactions on the reentrant condensation of disordered proteins. *Biomacromolecules* **2021**, *22*, 1532–1544.

(24) Roosen-Runge, F.; Heck, B. S.; Zhang, F.; Kohlbacher, O.; Schreiber, F. Interplay of pH and binding of multivalent metal ions: charge inversion and reentrant condensation in protein solutions. *The Journal of Physical Chemistry B* **2013**, *117*, 5777–5787.

(25) Krainer, G.; Welsh, T. J.; Joseph, J. A.; St George-Hyslop, P.; Hyman, A. A.; Collepardo-Guevara, R.; Alberti, S.; Knowles, T. P. Reentrant liquid condensate phase of proteins is stabilized by hydrophobic and non-ionic interactions. *Biophysical Journal* **2021**, *120*, 28a.

(26) Woldeyes, M. A.; Qi, W.; Razinkov, V. I.; Furst, E. M.; Roberts, C. J. How well do low- and high-concentration protein interactions predict solution viscosities of monoclonal antibodies? *Journal of Pharmaceutical Sciences* **2019**, *108*, 142–154.

(27) Valente, J. J.; Payne, R. W.; Manning, M. C.; Wilson, W. W.; Henry, C. S. Colloidal behavior of proteins: effects of the second virial coefficient on solubility, crystallization and aggregation of proteins in aqueous solution. *Current Pharmaceutical Biotechnology* **2005**, *6*, 427–436.

(28) Ho, J. G.; Middelberg, A. P.; Ramage, P.; Kocher, H. P. The likelihood of aggregation during protein renaturation can be assessed using the second virial coefficient. *Protein Science* **2003**, *12*, 708–716.

(29) Chi, E. Y.; Krishnan, S.; Kendrick, B. S.; Chang, B. S.; Carpenter, J. F.; Randolph, T. W. Roles of conformational stability and colloidal stability in the aggregation of recombinant human granulocyte colony-stimulating factor. *Protein Science* **2003**, *12*, 903–913.

(30) Eberstein, W.; Georgalis, Y.; Saenger, W. Molecular interactions in crystallizing lysozyme solutions studied by photon correlation spectroscopy. *Journal of Crystal Growth* **1994**, *143*, 71–78.

(31) Klement, K.; Wieligmann, K.; Meinhardt, J.; Hortschansky, P.; Richter, W.; Fändrich, M. Effect of different salt ions on the propensity of aggregation and on the structure of Alzheimer's Aβ (1-40) amyloid fibrils. *Journal of molecular biology* **2007**, *373*, 1321–1333.

(32) Owczarz, M.; Arosio, P. Sulfate anion delays the self-assembly of human insulin by modifying the aggregation pathway. *Biophysical Journal* **2014**, *107*, 197–207.

(33) Chaaban, H.; Vallooran, J. J.; van de Weert, M.; Fodera, V. Ion-mediated morphological

diversity in protein amyloid systems. *The Journal of Physical Chemistry Letters* **2022**, *13*, 3586–3593.

(34) Matsukuma, D.; Sambai, T.; Otsuka, H. UCST-type phase transition driven by protein-derived polypeptide employing gelatin and chitosan. *Polymers for Advanced Technologies* **2017**, *28*, 1636–1641.

(35) Blundell, T.; Dodson, G.; Hodgkin, D.; Mercola, D. Insulin: The Structure in the Crystal and its Reflection in Chemistry and Biology by. *Advances in Protein Chemistry* **1972**, *26*, 279–402.

(36) Nagel, N.; Graewert, M. A.; Gao, M.; Heyse, W.; Jeffries, C. M.; Svergun, D.; Berchtold, H. The quaternary structure of insulin glargine and glulisine under formulation conditions. *Biophysical chemistry* **2019**, *253*, 106226.

(37) Nielsen, L.; Khurana, R.; Coats, A.; Frokjaer, S.; Brange, J.; Vyas, S.; Uversky, V. N.; Fink, A. L. Effect of environmental factors on the kinetics of insulin fibril formation: elucidation of the molecular mechanism. *Biochemistry* **2001**, *40*, 6036–6046.

(38) Aliakseyeu, A.; Hlushko, R.; Sukhishvili, S. A. Nonionic star polymers with upper critical solution temperature in aqueous solutions. *Polymer Chemistry* **2022**, *13*, 2637–2650.

(39) Fennema Galparsoro, D.; Zhou, X.; Jaaloul, A.; Piccirilli, F.; Vetri, V.; Fodera, V. Conformational transitions upon maturation rule surface and pH-responsiveness of α-lactalbumin microparticulates. *ACS Applied Bio Materials* **2021**, *4*, 1876–1887.

(40) Foderà, V.; Vetri, V.; Wind, T. S.; Noppe, W.; Cornett, C.; Donald, A. M.; Morozova-Roche, L. A.; Vestergaard, B. Observation of the early structural changes leading to the formation of protein superstructures. *The Journal of Physical Chemistry Letters* **2014**, *5*, 3254–3258.

(41) Iadanza, M. G.; Jackson, M. P.; Hewitt, E. W.; Ranson, N. A.; Radford, S. E. A new era for understanding amyloid structures and disease. *Nature Reviews Molecular Cell Biology* **2018**, *19*, 755–773.

(42) Zhou, X.; Sinkjær, A. W.; Zhang, M.; Pinholt, H. D.; Nielsen, H. M.; Hatzakis, N. S.; van de Weert, M.; Fodera, V. Heterogeneous and Surface-Catalyzed Amyloid Aggregation Monitored by Spatially Resolved Fluorescence and Single Molecule Microscopy. *The Journal of Physical Chemistry Letters* **2023**, *14*, 912–919.

(43) Krebs, M. R.; MacPhee, C. E.; Miller, A. F.; Dunlop, I. E.; Dobson, C. M.; Donald, A. M. The formation of spherulites by amyloid fibrils of bovine insulin. *Proceedings of the National Academy of Sciences* **2004**, *101*, 14420–14424.

(44) Exley, C.; House, E.; Collingwood, J. F.; Davidson, M. R.; Cannon, D.; Donald, A. M. Spherulites of Amyloid-β 42 In Vitro and in Alzheimer's Disease. *Journal of Alzheimer's Disease* **2010**, *20*, 1159–1165.

(45) Vanysek, P. Thermochemistry, Electrochemistry, and Kinetics. *CRC Handbook of Chemistry and Physics. Boca Raton: Taylor and Francis Group LLC* **2008**, 5–76.

(46) Whittingham, J. L.; Scott, D. J.; Chance, K.; Wilson, A.; Finch, J.; Brange, J.; Dodson, G. G. Insulin at pH 2: structural analysis of the conditions promoting insulin fibre formation. *Journal of Molecular Biology* **2002**, *318*, 479–490.

(47) Gokarn, Y. R.; Fesinmeyer, R. M.; Saluja, A.; Razinkov, V.; Chase, S. F.; Laue, T. M.; Brems, D. N. Effective charge measurements reveal selective and preferential accumulation of anions, but not cations, at the protein surface in dilute salt solutions. *Protein Science* **2011**, *20*, 580–587.

(48) Fodera, V.; Librizzi, F.; Groenning, M.; van de Weert, M.; Leone, M. Secondary nucleation and accessible surface in insulin amyloid fibril formation. *The Journal of Physical Chemistry B* **2008**, *112*, 3853–3858.

(49) De Luca, G.; Galparsoro, D. F.; Sancataldo, G.; Leone, M.; Foderà, V.; Vetri, V. Probing ensemble polymorphism and single aggregate structural heterogeneity in insulin amyloid self-assembly. *Journal of Colloid and Interface Science* **2020**, *574*, 229–240.

(50) Cannon, D.; Eichhorn, S. J.; Donald, A. M. Structure of Spherulites in Insulin, β-Lactoglobulin, and Amyloid β. *ACS Omega* **2016**, *1*, 915–922.

(51) Qiang, W.; Yau, W.-M.; Lu, J.-X.; Collinge, J.; Tycko, R. Structural variation in amyloid-β fibrils from Alzheimer's disease clinical subtypes. *Nature* **2017**, *541*, 217–221.

(52) Vaquer-Alicea, J.; Diamond, M. I. Propagation of protein aggregation in neurodegenerative diseases. *Annual Review of Biochemistry* **2019**, *88*, 785–810.

(53) Yin, L.; Chen, X.; Tiwari, A.; Vicini, P.; Hickling, T. P.; others The role of aggregates of therapeutic protein products in immunogenicity: an evaluation by mathematical modeling. *Journal of Immunology Research* **2015**, *2015*.

(54) Hermeling, S.; Crommelin, D. J.; Schellekens, H.; Jiskoot, W. Structure-immunogenicity relationships of therapeutic proteins. *Pharmaceutical research* **2004**, *21*, 897–903.

(55) Thorlaksen, C.; Schultz, H. S.; Gammelgaard, S. K.; Jiskoot, W.; Hatzakis, N. S.; Nielsen, F. S.; Solberg, H.; Foderà, V.; Bartholdy, C.; Groenning, M. In vitro and in vivo immunogenicity assessment of protein aggregate characteristics. *International Journal of Pharmaceutics* **2023**, *631*, 122490.

(56) Cawood, E. E.; Karamanos, T. K.; Wilson, A. J.; Radford, S. E. Visualizing and trapping transient oligomers in amyloid assembly pathways. *Biophysical Chemistry* **2021**, *268*, 106505.

(57) Hopkins, J. B.; Gillilan, R. E.; Skou, S. BioXTAS RAW: improvements to a free open-

source program for small-angle X-ray scattering data reduction and analysis. *Journal of applied crystallography* **2017**, *50*, 1545–1553.

(58) Konarev, P. V.; Volkov, V. V.; Sokolova, A. V.; Koch, M. H.; Svergun, D. I. PRIMUS: a Windows PC-based system for small-angle scattering data analysis. *Journal of applied crystallography* **2003**, *36*, 1277–1282.

(59) Chang, X.; Jørgensen, A. M. M.; Bardrum, P.; Led, J. J. Solution structures of the R6 human insulin hexamer. *Biochemistry* **1997**, *36*, 9409–9422.

(60) Timofeev, V.; Chuprov-Netochin, R.; Samigina, V.; Bezuglov, V.; Miroshnikov, K.; Kuranova, I. X-ray investigation of gene-engineered human insulin crystallized from a solution containing polysialic acid. *Acta Crystallographica Section F: Structural Biology and Crystallization Communications* **2010**, *66*, 259–263.

(61) Manalastas-Cantos, K.; Konarev, P. V.; Hajizadeh, N. R.; Kikhney, A. G.; Petoukhov, M. V.; Molodenskiy, D. S.; Panjkovich, A.; Mertens, H. D.; Gruzinov, A.; Borges, C.; others ATSAS 3.0: expanded functionality and new tools for small-angle scattering data analysis. *Journal of applied crystallography* **2021**, *54*, 343–355.

(62) Smith, M. I.; Foderà, V.; Sharp, J. S.; Roberts, C. J.; Donald, A. M. Factors affecting the formation of insulin amyloid spherulites. *Colloids and Surfaces B: Biointerfaces* **2012**, *89*, 216–222.

(63) Křížková, K.; Veverka, V.; Maletínská, L.; Hexnerová, R.; Brzozowski, A. M.; Jiráček, J.; Žáková, L. Structural and functional study of the GlnB22-insulin mutant responsible for maturity-onset diabetes of the young. *PloS one* **2014**, *9*, e112883.

(64) Van Der Spoel, D.; Lindahl, E.; Hess, B.; Groenhof, G.; Mark, A. E.; Berendsen, H. J. GROMACS: fast, flexible, and free. *Journal of computational chemistry* **2005**, *26*, 1701–1718.

(65) Abraham, M. J.; Murtola, T.; Schulz, R.; Páll, S.; Smith, J. C.; Hess, B.; Lindahl, E. GROMACS: High performance molecular simulations through multi-level parallelism from laptops to supercomputers. *SoftwareX* **2015**, *1*, 19–25.

(66) Maier, J. A.; Martinez, C.; Kasavajhala, K.; Wickstrom, L.; Hauser, K. E.; Simmerling, C. ff14SB: improving the accuracy of protein side chain and backbone parameters from ff99SB. *Journal of chemical theory and computation* **2015**, *11*, 3696–3713.

(67) Baaden, M.; Berny, F.; Madic, C.; Wipff, G. M3+ lanthanide cation solvation by acetonitrile: The role of cation size, counterions, and polarization effects investigated by molecular dynamics and quantum mechanical simulations. *The Journal of Physical Chemistry A* **2000**, *104*, 7659–7671.

(68) Kashefolgheta, S.; Verde, A. V. Developing force fields when experimental data is sparse: AMBER/GAFF-compatible parameters for inorganic and alkyl oxoanions. *Physical Chemistry Chemical Physics* **2017**, *19*, 20593–20607.

(69) Zhang, J. The hybrid idea of (energy minimization) optimization methods applied to study prion protein structures focusing on the beta2-alpha2 loop. *Biochem Pharmacol (Los Angel)* **2015**, *4*, 2167–0501.

(70) Müller, K.; Brown, L. D. Location of saddle points and minimum energy paths by a constrained simplex optimization procedure. *Theoretica chimica acta* **1979**, *53*, 75–93.

(71) Bussi, G.; Donadio, D.; Parrinello, M. Canonical sampling through velocity rescaling. *The Journal of chemical physics* **2007**, *126*.

(72) Parrinello, M.; Rahman, A. Strain fluctuations and elastic constants. *The Journal of Chemical Physics* **1982**, *76*, 2662–2666.

(73) Parrinello, M.; Rahman, A. Crystal structure and pair potentials: A molecular-dynamics study. *Physical review letters* **1980**, *45*, 1196.

(74) Parrinello, M.; Rahman, A. Polymorphic transitions in single crystals: A new molecular dynamics method. *Journal of Applied physics* **1981**, *52*, 7182–7190.

(75) Nosé, S. A molecular dynamics method for simulations in the canonical ensemble. *Molecular physics* **1984**, *52*, 255–268.

(76) Nosé, S. A unified formulation of the constant temperature molecular dynamics methods. *The Journal of chemical physics* **1984**, *81*, 511–519.

(77) Nosé, S. An extension of the canonical ensemble molecular dynamics method. *Molecular Physics* **1986**, *57*, 187–191.

(78) Hoover, W. G. Canonical dynamics: Equilibrium phase-space distributions. *Physical review A* **1985**, *31*, 1695.

(79) Essmann, U.; Perera, L.; Berkowitz, M. L.; Darden, T.; Lee, H.; Pedersen, L. G. A smooth particle mesh Ewald method. *The Journal of chemical physics* **1995**, *103*, 8577–8593.

(80) Hess, B.; Bekker, H.; Berendsen, H. J.; Fraaije, J. G. LINCS: A linear constraint solver for molecular simulations. *Journal of computational chemistry* **1997**, *18*, 1463–1472.